Multigap electron-phonon superconductivity in the quasi-one-dimensional pnictide $K_2Mo_3As_3$

Bing-Hua Lei [1] and David J. Singh [1,2,*]

[1]*Department of Physics and Astronomy, University of Missouri, Columbia, Missouri 65211, USA*
[2]*Department of Chemistry, University of Missouri, Columbia, Missouri 65211, USA*

(Received 26 January 2021; accepted 11 March 2021; published 19 March 2021)

We show, using density functional calculations, that quasi-one-dimensional $K_2Mo_3As_3$, which is closely related to $K_2Cr_3As_3$ and has very similar superconducting properties, is not close to magnetism and has conventional *s* wave electron-phonon superconductivity. This superconductivity is of multigap character due to different coupling on different Fermi surface sheets. This is discussed in relation to the properties of this family of quasi-one-dimensional pnictide superconductors. The results show that this family of superconductors provides a unique opportunity for studying the interplay of spin fluctuations and electron-phonon superconductivity in transition metal pnictides, and offer a path for sorting out the different proposed superconducting scenarios in this fascinating family of pnictide superconductors.

DOI: 10.1103/PhysRevB.103.094512

The discovery of Fe-pnictide superconductors provided a new window into unconventional high temperature superconductivity [1]. These compounds, similar to cuprates, exhibit nearness to magnetism, layered structures with square planar transition element sheets and unconventional order parameters [2,3]. However, these are unlike cuprates in that the order parameter is different, as is the bonding arrangement. Importantly, the magnetism and nature of electron correlations both appear to be different [4,5]. More generally, progress in understanding superconductivity, especially unconventional superconductivity, has been driven by the discovery of new classes of superconducting materials. These include heavy Fermions, cuprates, Fe-based superconductors and the 4d transition metal oxide, Sr_2RuO_4 [6,7], all of which are superconductors near magnetism, but otherwise show quite different properties. Each of these has provided insights into the interplay between magnetism and superconductivity which, although long studied [8], remains one of the key challenges in developing understanding of unconventional superconductivity [9].

The $A_2T_3As_3$, where A is an alkali metal, are a class of pnictide superconductors [10], with chemical similarity to the iron-pnictide superconductors [1], which have high critical temperatures and may be examples of spin-fluctuation mediated superconductors [3,9,11]. The $A_2T_3As_3$ materials show signatures suggesting unconventional superconductivity. They differ from the Fe-based superconductors in that the structures are based on one dimensional transition metal tubes, coordinated by As. This is important, for example, because spin wave behavior and spin fluctuations generally depend strongly on dimensionality. Additionally, these materials are examples of noncentrosymmetric superconductors. Various pairing states have been proposed, including triplet states and recently topological superconducting behavior in connection with *p*-wave states [12]. Consistent with unconventional superconductivity, the NMR Hebel-Slichter peak is absent [13,14], the upper critical fields exceed the Pauli limit, and (at least in the Cr compounds) the renormalization of the electronic density of states inferred from specific heat measurements is high [10,15,16].

Superconductivity with similar T_c occurs for both T=Cr and T=Mo, with the Mo compounds showing somewhat higher T_c in general [17–19]. Specifically, the experimental T_c = 10.4 K, 10.5 K, and 11.5 K, for $K_2Mo_3As_3$, $Rb_2Mo_3As_3$, and $Cs_2Mo_3As_3$, respectively, as compared to 6.1 K, 4.8 K, and 2.2 K for the corresponding Cr compounds [10,20,21]. We note that persistence of superconductivity under substitution with a 4d element does not preclude spin-fluctuation induced unconventional superconductivity, as seen for example in the nearness to magnetism of Sr_2RuO_4, and the fact that Fe-based superconductivity persists up to ∼35% Ru substitution for Fe in $(Ba,Sr)(Fe,Ru)_2As_2$, and in fact superconductivity is induced by Ru alloying starting with stoichiometric $BaFe_2As_2$ [22,23]. Magnetism is less common in Mo compounds compared to Cr, but Mo moments are important in materials, for example in the room temperature ferromagnetism of double perovskite Sr_2FeMoO_6 [24]. They provide magnetism in other materials as well [25,26], and have been suggested as important in $K_2Mo_3As_3$ [10,20,21]. In any case, substitution of Mo for Cr provides a mechanism for tuning the magnetism, which may provide insights into the superconductivity, especially considering similarities between the anomalously high upper critical fields in both Mo and Cr compounds.

The $A_2Cr_3As_3$ superconductors show multisheet Fermi surfaces, with both one-dimensional (1D) and three-dimensional (3D) sections [27–31] and clear signatures of magnetism both from first principles calculations [27,28,31] and experiments [32]. These Cr compounds are close to ferromagnetism as well as antiferromagnetism. This is seen, for example, in ^{75}As nuclear quadrupole resonance (NQR) measurements, where it was found that substitutions on the alkali metal site tune the

*singhdj@missouri.edu

proximity to a ferromagnetic quantum critical point as well as the superconducting critical temperature [13,33]. Ferromagnetic fluctuations are generally destructive to standard *s*-wave superconductivity [8], and may favor triplet superconductivity [27,34]. analogous to proposals for Sr_2RuO_4 [35,36]. Neutron scattering measurements, which are more sensitive to antiferromagnetism, find spin fluctuations near (0,0,1/2), indicating a competition between ferromagnetic and antiferromagnetic states in this system [37].

However, the behavior of the Cr compounds is complicated by a structural instability of the Cr_3As_3 wires. This does not fully order, is affected by stoichiometry (including a tendency to take up H when K deficient), and does affect the magnetic, electronic, and superconducting behavior [38–41]. This leads to wide variety of proposed electronic and superconducting states, including evidence for Tomonaga-Luttinger liquid physics [42], spin-triplet superconductivity [34,43], topological superconductivity [12,44], and nodal gap functions [16,32,33,45].

Here, we use first-principles calculations to address the properties of $K_2Mo_3As_3$. This provides a unique opportunity for sorting out the various proposals for superconductivity in this family of compounds. We find that $K_2Mo_3As_3$ is very different from $K_2Cr_3As_3$. Unlike that compound, $K_2Mo_3As_3$ does not show phonon instabilities in the ideal hexagonal structure. This facilitates analysis of the magnetic and electronic properties. We find that the electronic structure is similar to that of $K_2Cr_3As_3$, with both 1D and 3D Fermi surface sheets. However, the magnetism is very different. We do not find proximity to ferromagnetism, nor do we find any ordered antiferromagnetic phase. The stability of the ideal structure enables electron phonon calculations. We find, remarkably, that the superconductivity of $K_2Mo_3As_3$ can be well described by standard electron-phonon theory, and additionally that it is a multigap superconductor, providing an explanation for the high observed upper critical field.

We did density functional theory (DFT) calculations with the Perdew, Burke, Ernzerhof generalized gradient approximation (PBE-GGA) [46], and the general potential linearized augmented planewave method as implemented in the WIEN2k code [47]. The lattice parameters of the fully relaxed structure are $a = 10.256$ Å, $c = 4.463$ Å, which are in good accord with the reported experimental values, $a = 10.145$ Å, $c = 4.453$ Å[18]. Emphasizing the connection of the Cr- and Mo-based compounds, we note that they show remarkably similar electronic structures, as seen in the Fermi surfaces of Fig. 1. Ideal structure $K_2Cr_3As_3$ shows two almost degenerate 1D Fermi surface sheets and a 3D sheet. The 3D sheet distorts, and the near degeneracy of the two 1D sheets is lifted with the structure distortion. $K_2Mo_3As_3$ similarly shows a 3D sheet and two 1D sheets, with changes in detail, particularly a lifting of the near degeneracy of the 1D sheets relative to $K_2Cr_3As_3$. The fractional band occupancies are 0.910 (γ), 0.609 (β), and 0.481 (α) for the 3D and the two 1D sheets in $K_2Mo_3As_3$, as compared to 0.868, 0.572, and 0.560 for ideal $K_2Cr_3As_3$ and 0.901, 0.615, and 0.484 for distorted $K_2Cr_3As_3$. The electronic density of states at the Fermi level for $K_2Mo_3As_3$ is $N(E_F) = 4.95$ eV^{-1}/f.u., with strong Mo d contributions. This is similar to be behavior of $K_2Cr_3As_3$, as noted previously [33].

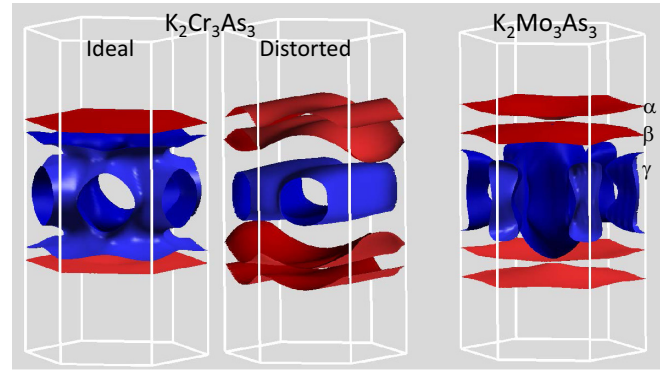

FIG. 1. Fermi surfaces of ideal and distorted $K_2Cr_3As_3$ and $K_2As_3Mo_3$, as obtained with the PBE-GGA functional. The labels of the Fermi surfaces for $K_2Mo_3As_3$ are as shown.

Turning to magnetism, the value of $N(E_F)$ is too small to lead to a Stoner instability towards ferromagnetism. With a reasonable Stoner parameter [48] of ~0.75 eV for 4d Mo, and three Mo per formula unit, a Stoner instability would require $N(E_F) \geqslant 8$ eV^{-1}/f.u., placing $K_2Mo_3As_3$ far from ferromagnetism. Figure 2 compares fixed spin moment calculations for $K_2Mo_3As_3$ with hexagonal $K_2Cr_3As_3$. $K_2Cr_3As_3$ shows a weak ferromagnetic instability, consistent with experiments showing proximity to ferromagnetism [13,44]. In contrast, $K_2Mo_3As_3$ does not show any such instability. We also find an instability for distorted $K_2Cr_3As_3$, but this is of ferrimagnetic nature, where different Cr atoms in the reduced symmetry cell take different moments, mixing ferromagnetism and antiferromagnetism. Tests for various possible collinear antiferromagnetic arrangements for $K_2Mo_3As_3$, as shown in the right panel of Fig. 2, show no magnetic instabilities, as anticipated from the Stoner picture. While the aggregate Fermi surface, which defines the low energy electronic structure, is 3D due to the γ sheet, there are 1D characteristics. True 1D correlated electronic systems can show instabilities, particularly charge density waves (manifested by phonon

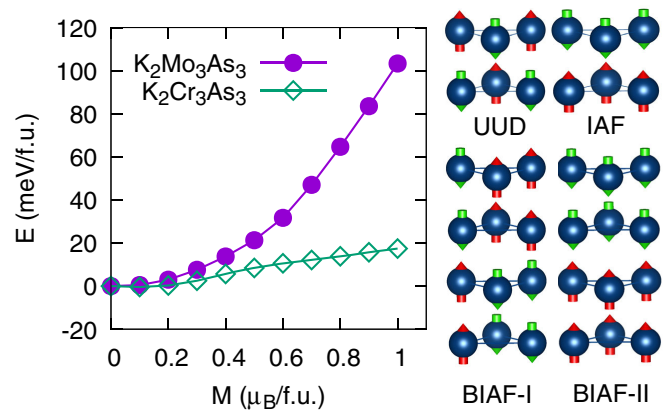

FIG. 2. Comparison of fixed spin moment energy as a function of spin magnetization for $K_2Mo_3As_3$ and $K_2Cr_3As_3$, obtained with the reported crystal structures and relaxed internal atomic coordinates (left panel). Collinear magnetic orders investigated showing the Mo atoms comprising a *c*-axis chain (right panel).

instabilities), spin density waves (manifested by magnetic ordering), and also instability of the Fermi liquid state [49,50]. As discussed below, we do not find phonon instabilities. Also, importantly, the magnetic configurations tested include two (BIAF-I and BIAF-II) with a doubled unit cell along the c axis, which corresponds closely to the expected nesting vector of the most 1D α Fermi surface sheet, which has a filling of 0.481, close to 0.5. Thus, $K_2Mo_3As_3$ is much further from magnetism than the Cr compounds.

Phonons, the Eliashberg function $\alpha^2F(\omega)$, and related parameters needed for T_c were obtained using the QUANTUM ESPRESSO and EPW codes, with the PBE-GGA and projector augmented wave pseudopotentials with nonlinear core corrections [51]. It is essential to have reliable phonon dispersions for this purpose. We used the EPW code [52–54] to extract the Eliashberg function $\alpha^2F(\omega)$, and band dependent gap values on the Fermi surface. We checked these by comparing the phonon dispersions obtained in QUANTUM ESPRESSO with those obtained by supercell calculations using the VASP code using different **q** meshes and energy cutoffs. These calculations showed stable phonons for $K_2Mo_3As_3$, in contrast to calculations for $K_2Cr_3As_3$ [38]. As a further test, we relaxed the crystal structure, starting with various low symmetry displacements of atoms in the unit cell. However, in all cases the structure relaxed back to the high symmetry hexagonal structure, also in contrast to the behavior of $K_2Cr_3As_3$. The relaxed lattice parameters for $K_2Mo_3As_3$ are a=10.256 Å, c=4.46 Å. The EPW calculations were done with a Wannier interpolated fine $36 \times 36 \times 48$ **k**-point grid based on data from a $18 \times 18 \times 24$ **q** grid. Convergence was tested by using different mesh sizes. The phonons were as obtained with QUANTUM ESPRESSO. The QUANTUM ESPRESSO force constants were used in the EPW calculation, so the phonons for these calculations are the same.

The phonon dispersion, phonon density of states $G(\omega)$, and Eliashberg spectral function $\alpha^2F(\omega)$ are given in Fig. 3. The integrated electron-phonon coupling constant $\lambda = 2\int(\alpha^2F(\omega)/\omega)d\omega$ is $\lambda = 1.92$. This yields a moderate mass renormalization of $m^*/m = (1+\lambda) = 2.92$ and puts $K_2Mo_3As_3$ in the strong coupling regime for electron-phonon superconductivity. The logarithmically averaged phonon frequency, $\omega_{\log} = \exp[(2/\lambda)\int(\alpha^2F(\omega)/\omega)\ln\omega d\omega]$ is $\omega_{\log} = 2.56$ THz $= 123$ K. The superconducting critical temperature can be obtained using the McMillan formula as modified by Allen and Dynes [55],

$$T_c = \frac{\omega_{\log}}{1.2}\exp\left[\frac{-1.04(1+\lambda)}{\lambda(1-0.62\mu^*)-\mu^*}\right]. \quad (1)$$

This yields predicted critical temperatures of 16.4 K and 15.2 K using reasonable values of the Coulomb repulsion parameter, $\mu^* = 0.12$ and 0.15, respectively. These values are somewhat higher than the experimental value of 10.4 K, perhaps reflecting scattering due to spin fluctuations.

It may be noted that there is a sizable peak in $\alpha^2F(\omega)$ at ~1.8 THz. This comes from phonons with primarily Mo character that modulate the Mo-Mo distances in the tubes. In addition, there are significant contributions for higher frequency modes extending to the top of the phonon spectrum. The resulting $\omega_{\log} = 2.6$ THz reflects these higher frequency contributions, which contribute to the T_c.

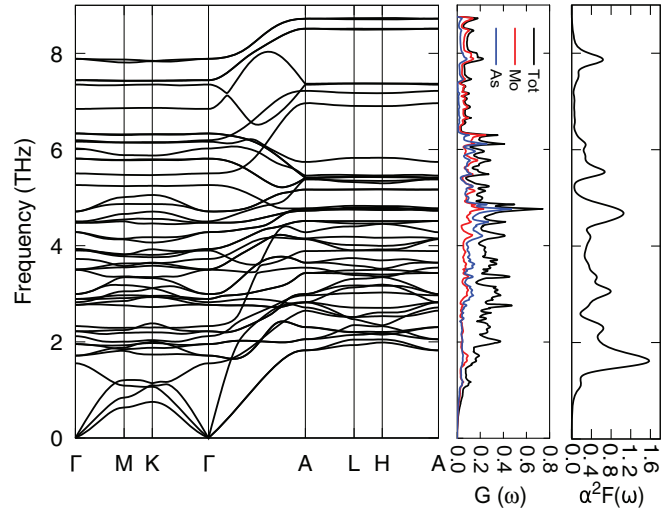

FIG. 3. Calculated phonon dispersions of $K_2Mo_3As_3$. Left–the phonon density of states, $G(\omega)$. Middle–projections of Mo and As character. Right–calculated electron-phonon $\alpha^2F(\omega)$. A smoothing was applied to the density of states and electron phonon curves.

Thus, $K_2Cr_3As_3$ is well described as an electron-phonon superconductor that is not in proximity to magnetism, but that does have a multisheet Fermi surface with 1D and 3D sections. As mentioned, experiments show upper critical fields H_{c2} that significantly exceed the Pauli limit in these materials. This is characteristic of two gap superconductivity within a standard electron-phonon scenario [56–60]. We calculated the gap on the different Fermi surface sheets (see Fig. 1) using EPW. The resulting average gap values are $\Delta_\alpha = 2.3$ meV, $\Delta_\beta = 4.8$ meV, and $\Delta_\gamma = 4.0$ meV for the α, β, and γ sheets, respectively. Thus, there is a considerable gap anisotropy, with much weaker pairing on the isolated 1D α sheet as compared to the 3D γ sheet and the 1D β sheet near it. The gap values Δ are significantly higher than the weak coupling BCS value $\Delta_{\rm BCS} = 1.764k_BT_c$. This reflects the strong coupling mentioned above. These results show a multigap superconducting scenario, which explains the high upper critical fields seen in this compound.

This leaves three scenarios for $A_2T_3As_3$ superconductivity that are compatible with experiments and the above results. These can be distinguished based on the phase diagram, especially the properties of the alloy, $K_2(Cr_{1-x}Mo_x)_3As_3$ as shown schematically in Fig. 4. This connects the endpoint compounds $K_2Mo_3As_3$ which, as shown above, is a multigap electron-phonon superconductor that is based on a Fermi liquid away from magnetism, and $K_2Cr_3As_3$, which is a superconductor with strong signatures of spin fluctuations.

Scenario 1: Both are electron-phonon superconductors. Spin fluctuations in $K_2Cr_3As_3$ suppress T_c, while enhancing the effective mass and electron scattering. Defining $\lambda_{\rm ep}$ as the electron phonon coupling, and $\lambda_{\rm sf}$ as the analogous coupling to mostly ferromagnetic, and therefore pair breaking, spin-fluctuations, the simplest model has the coupling for s-wave superconductivity as $\lambda_{sc} = \lambda_{\rm ep}$-$\lambda_{\rm sf}$ and specific heat mass enhancement, $\gamma/\gamma_{\rm bare} = 1 + \lambda_{\rm dos} = 1 + \lambda_{\rm ep} + \lambda_{\rm sf}$. The value of T_c is expected to increase monotonically with Mo content in $K_2(Cr_{1-x}Mo_x)_3As_3$, while renormalization and other

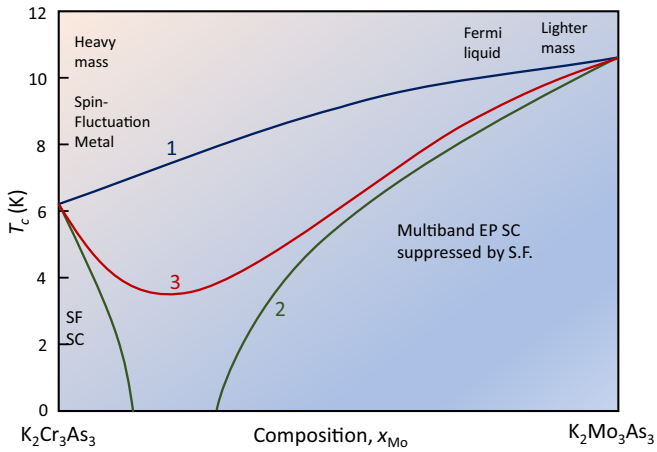

FIG. 4. Three scenarios for superconductivity (see text) and the phase diagram of the $K_2Cr_3As_3$–$K_2Mo_3As_3$ alloy system that are compatible with the present results and the existing experimental data.

signatures of magnetism decrease. H_{c2} exceeding the Pauli limit would exist across the phase diagram, reflecting multigap superconductivity.

Scenario 2: $K_2Cr_3As_3$ is an unconventional superconductor with spin-fluctuation pairing. In this case superconductivity may be sensitive to paramagnetic impurity scattering and the proximity to the magnetic critical point. T_c is expected to decrease with Mo alloying and vanish. Emergence of *s*-wave electron-phonon mediated superconductivity is at a higher concentration. The non-superconducting region in between would be analogous to Pd metal, which would be a superconductor without the destructive effect of spin fluctuations [8,61].

Scenario 3: There is a crossover regime between unconventional spin-fluctuation paired $K_2Cr_3As_3$ and *s*-wave electron-phonon paired $K_2Mo_3As_3$. Such a crossover could be between symmetry compatible superconducting states, e.g., sign-changing and non-sign-changing *s*-wave states, or even more interestingly between a triplet and a singlet state, which can be mixed in noncentrosymmetric materials. It could also be due to a phase separation, either chemical or a nanoscale electronic inhomogeneity as in striped phases of cuprates.

Importantly, the present results show that $K_2Mo_3As_3$ is a nonmagnetic electron-phonon multiband superconductor, and based on this the alloy phase diagrams can shed considerable light on the question of the origin and nature of superconductivity in the $K_2T_3As_3$ materials. The results thus enable sorting out the different proposed superconducting scenarios in this fascinating family of pnictide superconductors.

This work was supported by the US Department of Energy, Office of Science, Office of Basic Energy Sciences, Award No. DE-SC0019114. We are grateful for helpful discussions with Keith Taddei.

[1] Y. Kamihara, T. Watanabe, M. Hirano, and H. Hosono, J. Am. Chem. Soc. **130**, 3296 (2008).
[2] D. C. Johnston, Adv. Phys. **59**, 803 (2010).
[3] I. I. Mazin, D. J. Singh, M. D. Johannes, and M. H. Du, Phys. Rev. Lett. **101**, 057003 (2008).
[4] P. Dai, Rev. Mod. Phys. **87**, 855 (2015).
[5] M. M. Qazilbash, J. J. Hamlin, R. E. Baumbach, L. Zhang, D. J. Singh, M. B. Maple, and D. N. Basov, Nat. Phys. **5**, 647 (2009).
[6] Y. Maeno, H. Hashimoto, K. Yoshida, S. Nishizaki, T. Fujita, J. G. Bednorz, and F. Lichtenberg, Nature **372**, 532 (1994).
[7] A. Pustagow, Y. Luo, A. Chronister, Y. S. Su, D. A. Sokolov, F. Jezembeck, A. P. Mackenzie, C. W. Hicks, N. Kikugawa, S. Raghu, E. D. Bauer, and S. E. Brown, Nature **574**, 72 (2019).
[8] N. F. Berk and J. R. Schrieffer, Phys. Rev. Lett. **17**, 433 (1966).
[9] D. J. Scalapino, Rev. Mod. Phys. **84**, 1383 (2012).
[10] J. K. Bao, J. Y. Liu, C. W. Ma, Z. H. Meng, Z. T. Tang, Y. L. Sun, H. F. Zhai, H. Jiang, H. Bai, C. M. Feng, Z. A. Xu, and G. H. Cao, Phys. Rev. X **5**, 011013 (2015).
[11] K. Kuroki, S. Onari, R. Arita, H. Usui, Y. Tanaka, H. Kontani, and H. Aoki, Phys. Rev. Lett. **101**, 087004 (2008).
[12] C. C. Liu, C. Lu, L. D. Zhang, X. Wu, C. Fang, and F. Yang, Phys. Rev. Research **2**, 033050 (2020).
[13] J. Luo, J. Yang, R. Zhou, Q. G. Mu, T. Liu, Z. A. Ren, C. J. Yi, Y. G. Shi, and G. Q. Zheng, Phys. Rev. Lett. **123**, 047001 (2019).
[14] H. Z. Zhi, T. Imai, F. L. Ning, J. K. Bao, and G. H. Cao, Phys. Rev. Lett. **114**, 147004 (2015).
[15] T. Kong, S. L. Bud'ko, and P. C. Canfield, Phys. Rev. B **91**, 020507(R) (2015).
[16] Y. T. Shao, X. X. Wu, L. Wang, Y. G. Shi, J. P. Hu, and J. L. Luo, EPL **123**, 57001 (2018).
[17] Q. G. Mu, B. B. Ruan, K. Zhao, B. J. Pan, T. Liu, L. Shan, G. F. Chen, and Z. A. Ren, Sci. Bull. **63**, 952 (2018).
[18] K. Zhao, Q. G. Mu, B. B. Ruan, M. H. Zhou, Q. S. Yang, T. Liu, B. J. Pan, S. Zhang, G. F. Chen, and Z. A. Ren, Chin. Phys. Lett. **37**, 097401 (2020).
[19] K. Zhao, Q. G. Mu, B. B. Ruan, T. Liu, B. J. Pan, M. H. Zhou, S. Zhang, G. F. Chen, and Z. A. Ren, APL Mater. **8**, 031103 (2020).
[20] Z. T. Tang, J. K. Bao, Y. Liu, Y. L. Sun, A. Ablimit, H. F. Zhai, H. Jiang, C. M. Feng, Z. A. Xu, and G. H. Cao, Phys. Rev. B **91**, 020506(R) (2015).
[21] Z. T. Tang, J. K. Bao, Z. Wang, H. Bai, H. Jiang, Y. Liu, H. F. Zhai, C. M. Feng, Z. A. Xu, and G. H. Cao, Sci. China Mater. **58**, 16 (2015).
[22] W. Schnelle, A. Leithe-Jasper, R. Gumeniuk, U. Burkhardt, D. Kasinathan, and H. Rosner, Phys. Rev. B **79**, 214516 (2009).
[23] S. Sharma, A. Bharathi, S. Chandra, V. R. Reddy, S. Paulraj, A. T. Satya, V. S. Sastry, A. Gupta, and C. S. Sundar, Phys. Rev. B **81**, 174512 (2010).
[24] K. I. Kobayashi, T. Kimura, H. Sawada, K. Terakura, and Y. Tokura, Nature **395**, 677 (1998).
[25] Z. Guguchia, A. Kerelsky, D. Edelberg, S. Banerjee, F. von Rohr, D. Scullion, M. Augustin, M. Scully, D. A. Rhodes, Z. Shermadini, H. Luetkens, A. Shengelaya, C. Baines,

E. Morenzoni, A. Amato, J. C. Hone, R. Khasanov, J. L. Billinge, E. Santos, A. N. Pasupathy, and Y. J. Uemura, Sci. Adv. **4**, eaat3672 (2018).
[26] J. A. Hagmann, S. T. Le, L. F. Schneemeyer, J. A. Stroscio, T. Besara, J. Sun, D. J. Singh, T. Siegrist, D. G. Seiler, and C. A. Richter, Nanoscale **9**, 7922 (2017).
[27] X. X. Wu, C. C. Le, J. Yuan, H. Fan, and J. P. Hu, Chin. Phys. Lett. **32**, 057401 (2015).
[28] H. Jiang, G. Cao, and C. Cao, Sci. Rep. **5**, 16054 (2015).
[29] A. Subedi, Phys. Rev. B **92**, 174501 (2015).
[30] Y. Zhou, C. Cao, and F. C. Zhang, Sci. Bull. **62**, 208 (2017).
[31] L. D. Zhang, X. Zhang, J. J. Hao, W. Huang, and F. Yang, Phys. Rev. B **99**, 094511 (2019).
[32] D. Adroja, A. Bhattacharyya, M. Smidman, A. Hillier, Y. Feng, B. Pan, J. Zhao, M. R. Lees, A. Strydom, and P. K. Biswas, J. Phys. Soc. Japan **86**, 044710 (2017).
[33] Y. Yang, S. Q. Feng, H. Y. Liu, W. S. Wang, and Z. P. Chen, J. Supercond. Nov. Magn. **32**, 2421 (2019).
[34] X. Wu, F. Yang, C. Le, H. Fan, and J. Hu, Phys. Rev. B **92**, 104511 (2015).
[35] T. M. Rice and M. Sigrist, J. Phys.: Condens. Matter **7**, L643 (1995).
[36] I. I. Mazin and D. J. Singh, Phys. Rev. Lett. **79**, 733 (1997).
[37] K. M. Taddei, Q. Zheng, A. S. Sefat, and C. de la Cruz, Phys. Rev. B **96**, 180506(R) (2017).
[38] K. M. Taddei, G. Xing, J. Sun, Y. Fu, Y. Li, Q. Zheng, A. S. Sefat, D. J. Singh, and C. de la Cruz, Phys. Rev. Lett. **121**, 187002 (2018).
[39] G. Xing, L. Shang, Y. Fu, W. Ren, X. Fan, W. Zheng, and D. J. Singh, Phys. Rev. B **99**, 174508 (2019).
[40] K. M. Taddei, L. D. Sanjeewa, B. H. Lei, Y. Fu, Q. Zheng, D. J. Singh, A. S. Sefat, and C. dela Cruz, Phys. Rev. B **100**, 220503(R) (2019).
[41] S. Q. Wu, C. Cao, and G. H. Cao, Phys. Rev. B **100**, 155108 (2019).
[42] M. D. Watson, Y. Feng, C. W. Nicholson, C. Monney, J. M. Riley, H. Iwasawa, K. Refson, V. Sacksteder, D. T. Adroja, J. Zhao, and M. Hoesch, Phys. Rev. Lett. **118**, 097002 (2017).
[43] H. Zhong, X. Y. Feng, H. Chen, and J. Dai, Phys. Rev. Lett. **115**, 227001 (2015).
[44] C. Xu, N. Wu, G. X. Zhi, B. H. Lei, X. Duan, F. Ning, C. Cao, and Q. Chen, npj Comput. Mater. **6**, 30 (2020).
[45] D. T. Adroja, A. Bhattacharyya, M. Telling, Y. Feng, M. Smidman, B. Pan, J. Zhao, A. D. Hillier, F. L. Pratt, and A. M. Strydom, Phys. Rev. B **92**, 134505 (2015).
[46] J. P. Perdew, K. Burke, and M. Ernzerhof, Phys. Rev. Lett. **77**, 3865 (1996).
[47] P. Blaha, K. Schwarz, F. Tran, R. Laskowski, G. K. H. Madsen, and L. D. Marks, J. Chem. Phys. **152**, 074101 (2020).
[48] E. Sasioglu, C. Friedrich, and S. Blugel, Phys. Rev. B **83**, 121101(R) (2011).
[49] F. D. M. Haldane, J. Phys. C: Solid State Phys. **14**, 2585 (1981).
[50] J. Voit, Rep. Prog. Phys. **58**, 977 (1995).
[51] A. Dal Corso, Phys. Rev. B **81**, 075123 (2010).
[52] F. Giustino, M. L. Cohen, and S. G. Louie, Phys. Rev. B **76**, 165108 (2007).
[53] E. R. Margine and F. Giustino, Phys. Rev. B **87**, 024505 (2013).
[54] S. Ponce, E. R. Margine, C. Verdi, and F. Giustino, Computer Phys. Commun. **209**, 116 (2016).
[55] P. B. Allen and R. C. Dynes, Phys. Rev. B **12**, 905 (1975).
[56] A. Gurevich, Phys. Rev. B **67**, 184515 (2003).
[57] A. Gurevich, S. Patnaik, V. Braccini, K. H. Kim, C. Mielke, X. Song, L. D. Cooley, S. D. Bu, D. M. Kim, J. H. Choi, L. J. Belenky, J. Giencke, M. K. Lee, W. Tian, X. Q. Pan, A. Sin, E. E. Hellstrom, C. B. Eom, and D. C. Larbalestier, Supercond. Sci. Tech. **17**, 278 (2004).
[58] A. Gurevich, Phys. Rev. B **82**, 184504 (2010).
[59] F. Hunte, J. Jaroszynski, A. Gurevich, D. C. Larbalestier, R. Jin, A. S. Sefat, M. A. McGuire, B. C. Sales, D. K. Christen, and D. Mandrus, Nature **453**, 903 (2008).
[60] M. Zehetmayer, Supercond. Sci. Technol. **26**, 043001 (2013).
[61] K. H. Bennemann and J. W. Garland, Z. Phys. **260**, 367 (1973).